Magnetic and Electronic Structure Studies of Nanocrystalline $(Co_2Mn)_{40}Ni_{60}$ Alloy

N. Dadda[a,*], K. Dadda[b], W. Bouchelaghem[c], M. Medjaldi[d], S. Alleg[b], M. Bououdina[e] and E.K. Hlil[f]

[a] *Laboratoire de Synthèse et Biocatalyse Organique (LSBO), Département de Chimie, Université Badji Mokhtar Annaba, B.P. 12, Annaba 23000, Algeria*
[b] *Laboratoire de Magnétisme et Spectroscopie des Solides (LM2S), Département de Physique, Université Badji Mokhtar Annaba, B.P. 12, Annaba 23000, Algeria*
[c] *Laboratoire de Chimie des Matériaux Inorganiques, Département de Chimie, Université Badji Mokhtar Annaba, B.P. 12, Annaba 23000, Algeria*
[d] *Département Génie Industriel, Faculté des Sciences et Technologie, Université Abbes Laghrour Khenchela, Khenchela 40000, Algeria*
[e] *Department of Physics, College of Science, University of Bahrain, PO Box 32038, Kingdom of Bahrain*
[f] *Université Grenoble Alpes, CNRS, Grenoble INP, Institut Néel, 38000 Grenoble, France*

Received: 15.04.2021 & Accepted: 01.07.2021

Doi: 10.12693/APhysPolA.140.153 *e-mail: daddanaouri@yahoo.fr

Nanocrystalline $(Co_2Mn)_{40}Ni_{60}$ (wt%) alloy powder was prepared by high-energy ball milling under an argon atmosphere. Structure, microstructure, and magnetic properties were investigated by means of X-ray diffraction, scanning electron microscopy, and vibrating sample magnetometry. The X-ray diffraction analysis indicates that after 30 h of milling, a highly disordered (Co, Mn, Ni) solid solution emerges, having an average crystallite size of around 60 nm and a lattice parameter of about 3.5411 Å. Magnetization-field curves indicate the existence of ferromagnetic behavior irrespective of the milling time with a low hysteresis loop, a typical characteristic of a soft magnetic material. The magnetic properties, however, are found to be sensitive to the milling time: i.e. the ratio M_r/M_{sat} manifests the formation of multi-domains magnetic structure. Diverse magnetic parameters were acquired from the approach to magnetic saturation. The electronic structure of the ferromagnetic $(Co_2Mn)_{40}Ni_{60}$ alloy performed by self-consistent *ab initio* calculations based on the Korringa–Kohn–Rostocker method combined with the coherent potential approximation, reveals that the total DOS is mainly due to the 3*d*-like states of the constituent elements Mn, Co and Ni.

topics: ball milling, Ni–Co–Mn powder mixture, magnetic properties, electronic structure calculation

1. Introduction

Nanometals exhibit several physicochemical properties due to their hardness, small crystallite size, large surface area, varying morphology, mechanical strength, and interesting magnetic properties. Owing to the above characteristics, magnetic nanostructured materials were used in numerous fields such as magnetic recording [1], ferrofluids [2], magnetic resonance imaging [3], and magnetocaloric effect [4]. The magnetic behavior in nanostructured alloys based on transition metals is mainly governed by the magnetic anisotropy that depends on the chemical composition and the shape of samples. Furthermore, structural, magnetic and electronic properties of the magnetic multi-constituent alloys exhibit interesting properties, usually associated with the local ordering and interactions among the different components.

Many previous researches have been performed to study Ni–Mn [5, 6], Co–Mn [7, 8], and Ni–Co [9, 10] binary systems. Recently, Zhou et al. [11] performed a comprehensive study on the phase transformation and the magnetic properties of twenty two (22) compositions of a Ni–Co–Mn system prepared by arc melting with subsequent homogenization by annealing at 1000 °C for 24–72 h. The XRD results show that all samples have a face-centered-cubic (fcc) structure.

The Ni–Co–Mn alloy was synthesized by the mechanical alloying technique. This technique is considered a suitable route to produce different types of amorphous, nanocrystalline, composite, solid solution, and intermetallic compounds [10, 12–14]. Mechanical alloying is a solid-state powder processing method which is characterized by repeated fracturing, cold welding, and powder's agglomeration. The strong impact ball-powder-vials and/or impact ball-powder-ball involve plastic deformations of particles that reduce their size and enhance the structural defects. This modifies the physical, magnetic, and chemical properties in comparison to the coarse grain counterparts.

The present paper is devoted to the preparation of a nanocrystalline powdered (Co, Mn, Ni) solid solution by mechanical alloying. In the literature, the same ternary alloy was prepared by the melting technique. The alloy composition was mainly Co_2Mn mixed with 60% Ni in order to obtain a solid solution as both Co and Ni elements have a tendency to easily form solid solutions as compared to Mn. The disordered magnetic CoMn-base alloys having an fcc crystal structure are potential candidates for magnetic amplifier devices with the switched-mode power supply characterized by a soft magnetic behavior [15].

Previously, the phase transition and the magnetic properties of a Co–Mn system have been studied [16, 17]. Our research focuses particularly on the influence of milling on the evolution of the phase composition, structural and microstructural parameters, and subsequently the magnetic properties of $(Co_2Mn)_{40}Ni_{60}$ powder mixture. Additionally, the magnetic anisotropy is discussed and *ab initio* electronic structure calculations based on the KKR-CPA method are performed to study the magnetic and electronic structures of the selected composition that are considered as a chemical disordered system. The as-fabricated nanocrystalline alloy having a single solid solution and revealing a soft magnetic behavior can be used for magnetic amplifiers.

2. Experimental part

Nanocrystalline $(Co_2Mn)_{40}Ni_{60}$ (wt%) powders were prepared by a planetary ball mill (Fritsh Pulversitte 7) at 400 rpm under argon atmosphere at ambient temperature, from elemental Co (99.5%), Mn (99.95%) and Ni (99.9%) powders. The ball-to-powder weight ratio (BPR) was 23/1. The milling process was interrupted every 30 min for 15 min to avoid an excessive increase of the temperature inside the jars. The structure and microstructure were checked by X-ray diffraction (XRD) on a PANalytical Empyrean diffractometer in a (θ–θ) Bragg–Brentano geometry using Cu K_α radiation ($\lambda_{Cu} = 1.54056$ Å), and scanning electron microscopy (SEM) FEI Quantum 250. Magnetic measurements were carried out by a vibrating sample magnetometer (VSM) LakeShore 7404 at room temperature under an external magnetic field of 20 kOe. Some fundamental magnetic parameters were extracted from the approach to magnetic saturation.

3. Electronic structure calculation

To solve the density functional theory (DFT), we have used the KKR-CPA method [18] taking into consideration the parameterization of Vosko, Wilk, and Nusair (VWN) [19]. The form of the crystal potential was approached by muffin-tin potential, the wave functions were extended using an angular momentum quantum number up to $l = 2$, and the K-points' number in the first Brillouin zone was taken up to 144. The present calculations were carried out using a MACHIKANEYAMA2002v08 package produced by Akai of Osaka University [20].

4. Results and discussion

4.1. Crystal structure analysis

The evolution of the XRD patterns of $(Co_2Mn)_{40}Ni_{60}$ powder mixture as a function of the milling time is depicted in Fig. 1. The XRD pattern before milling (0 h) displays the diffraction peaks of elemental Ni with an fcc structure ($a = 3.524$ Å), Mn with a body centered cubic structure — bcc ($a = 8.905$ Å) and both allotropic forms of Co, namely a hexagonal compact — hcp ($a = 2.510$ Å and $c = 4.070$ Å) and fcc ($a = 3.550$ Å). As milling of the powder mixture progresses, the diffraction peaks become broader and their relative intensity is drastically reduced, some peaks disappear as well as there is a shift in the peaks' position.

This can be attributed to several phenomena occurring simultaneously during the milling process, including: (i) dissolution of one element into another host lattice, (ii) formation of nanocrystalline amorphous or semi-amorphous phases,

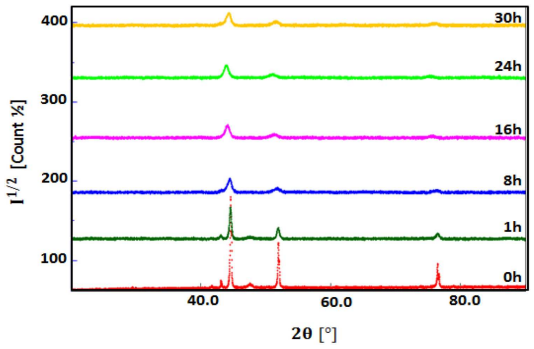

Fig. 1. Evolution of the XRD patterns of the ball-milled $(Co_2Mn)_{40}Ni_{60}$ powder mixture as a function of milling time.

TABLE I

Evolution of phase composition, lattice parameters (a and c), average crystallite size ($\langle L \rangle$) microstrains ($\langle \sigma^2 \rangle^{1/2}$) of ball-milled $(Co_2Mn)_{40}Ni_{60}$ powder mixture as a function of milling time.

t [h]	Phases	Phase composition [%] ± 1	a [Å] $\pm 10^{-3}$	c [Å] $\pm 10^{-3}$	$\langle L \rangle$ [nm] ± 1	$\langle \sigma^2 \rangle^{1/2}$ [%] $\pm 10^{-2}$
1	Ni	31.0	3.5226	–	36.4	0.081
	Mn	24.5	8.9094	–	99	0.091
	Co-hcp	45.5	2.5070	4.0651	164	0.093
8	SS-1	69.0	3.5400	–	31	0.465
	SS-2	31.0	2.4922	4.0702	46.5	0.250
16	SS(fcc)	100	3.5817	–	82	0.469
24	SS(fcc)	100	3.5632	–	63.5	1.150
30	SS(fcc)	100	3.5411	–	59.5	1.250

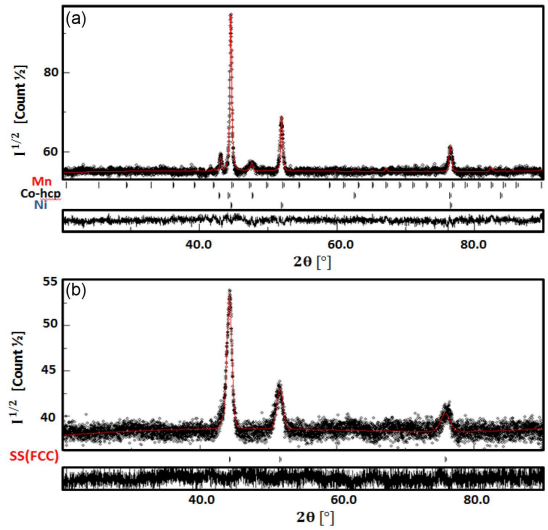

Fig. 2. Rietveld refinements of the XRD patterns of the ball-milled $(Co_2Mn)_{40}Ni_{60}$ powder mixture for: (a) 1 h (Sig = 1.052, $R_{wp}(\%) = 2.164$, $R_b(\%) = 1.728$, $R_{exp}(\%) = 1.874$), and (b) 30 h (Sig = 1.057, $R_{wp}(\%) = 2.091$, $R_b(\%) = 1.652$, $R_{exp}(\%) = 1.971$).

(iii) reduction of particle size known as grain refinement to the nanometer scale, (iv) formation of structural imperfections such as stacking faults, dislocations, vacancies resulting in the increase of microstrains.

The refinements of the recorded XRD patterns have been performed by means of MAUD software based on the Rietveld method [21], as shown in Fig. 2, and the refined parameters are reported in Table I. After 1 h of milling, the best refinement is achieved with the presence of the starting elements namely Co, Mn, and Ni (Fig. 2a). However, further milling up to 8 h reveals the formation of two solid solutions (SSs): SS-1 with an fcc structure (Fm-$3m$) in equilibrium with a second SS-2 having an hcp structure ($P6_3/mmc$) in the proportion of 69% and 31%, respectively. Thus, mechanical alloying is an easy process to produce solid solution phases. Much longer milling time up to 16 h results in the formation of a single solid solution phase (Co, Mn, Ni) labelled SS(cfc) (space group Fm-$3m$), see Table I. Similarly, at 30 h of milling (Fig. 2b), no significant modifications occurred, except changes in the values of structural and microstructural parameters (see Table I). Knowing that the MAUD program adopts an iterative least-square procedure to minimize the difference between the observed and simulated powder diffraction pattern, and the minimization was carried out by using the reliability index parameters; R_{wp} (weighted residual error), R_b (Bragg factor), and R_{exp} (expected error). The goodness of fit, Sig, is deduced by comparing R_{wp} with R_{exp}.

Figure 3 represents the variation of the proportion of the fcc solid solution (Fig. 3a), the average crystallite size $\langle L \rangle$ and the microstrain $\langle \sigma^2 \rangle^{1/2}$ (Fig. 3b), and the lattice parameter a as a function of the milling time (Fig. 3c). It can be observed that with the progress of milling, the phase proportion shows two states: (i) an increase from 8 h to 16 h due to the dissolution of Co and Mn elements within the Ni matrix, (ii) a constant variation from 16 h till 30 h due to the homogeneity of the chemical composition. Surprisingly, the value of the crystallite size increases significantly after 16 h representing the first stage of the milling process, characterized by the formation of the SS (Mn, Co, Ni). Once this SS phase is formed, the crystallite size reduces due to grain refinements. For the microstrain, it remains unchanged during the first stage of the formation of the SS phase and then it increases significantly for further milling.

The lattice parameter of the SS phase increases drastically during the first stage up to 16 h and then reduces gradually with further milling to reach a close value at 8 h. Based on the atomic radii of Ni (0.149 nm) Co (0.152 nm) and Mn (0.161 nm), the formation of the SS phase will occur progressively as follows: (i) Mn will dissolve firstly into the Ni host lattice followed by the lattice expansion since Mn

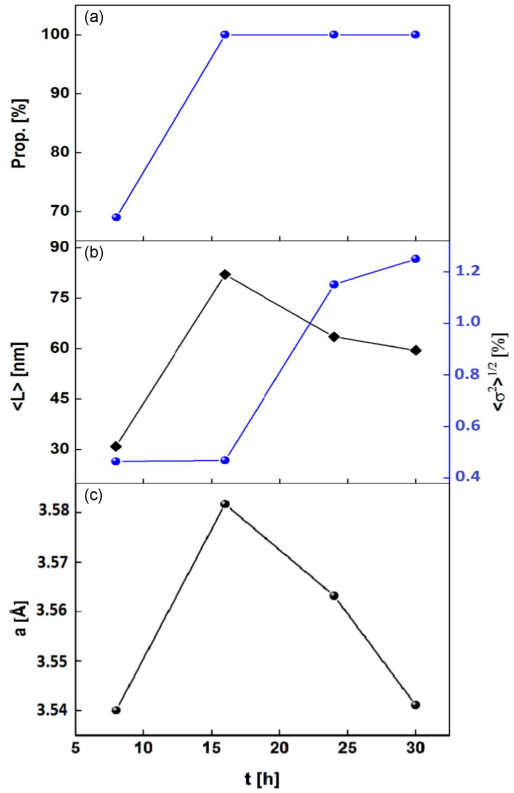

Fig. 3. Variation of (a) the fcc solid solution's proportion (Prop.), (b) average crystallite size ($\langle L \rangle$) and microstrains ($\langle \sigma^2 \rangle^{1/2}$), (c) lattice parameter a of the ball-milled $(Co_2Mn)_{40}Ni_{60}$ powder mixture as a function of milling time.

is much larger than Ni forming a primary (Ni, Mn) SS phase; (ii) subsequently, Co will dissolve into the already formed (Mn, Ni) SS to form the ternary (Co, Mn, Ni) SS phase followed by a lattice contraction since Co has a smaller atomic radius.

4.2. Morphological observations

Figure 4 displays SEM images of the (Co, Mn, Ni) powder mixture milled at different periods of time.

Before milling, both Ni and Co powder particles are fine spherical and rounded shapes, whereas Mn particles have different shapes and larger size. Since the particles are mostly soft, their tendency to weld and agglomerate together to form larger particles is highly probable. Moreover, the $(Co_2Mn)_{40}Ni_{60}$ powder mixture contains ductile and malleable particles of Ni, Co and Mn, therefore, the three elements have a strong tendency to form agglomerates. This is in good agreement with the XRD analysis, since during the first stage of the formation of (Co, Mn, Ni) SS phase, a significant increase in the crystallite size (from 31 nm up to 82 nm) has been observed (Table I and Fig. 3b). The same feature was observed in Cu–Fe–Co alloy [22]. Due to the hard impacts of the ball-powder-ball, the particle size is reduced after 30 h of milling; known as grain refinement following the phase formation and

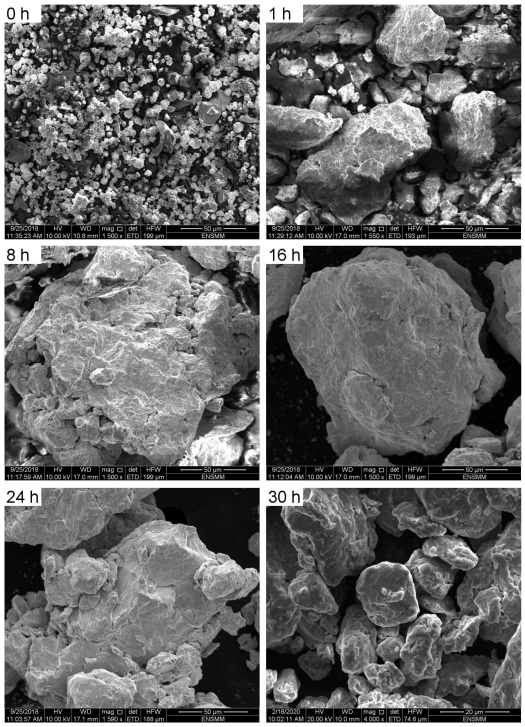

Fig. 4. SEM of the milled $(Co_2Mn)_{40}Ni_{60}$ powder mixture as a function of milling time.

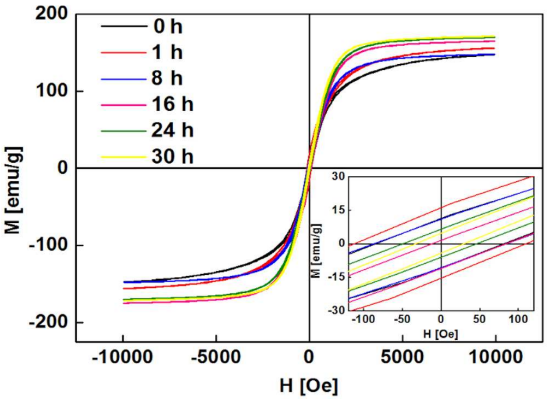

Fig. 5. Magnetization-field (M–H) curves of the ball-milled $(Co_2Mn)_{40}Ni_{60}$ powder mixture as a function of milling time. The inset shows a zoom in the lower field range.

as evaluated by the XRD analysis; i.e. a gradual decrease of crystallite size from 82 nm to 59 nm. Thus, cold soldering is the dominant process in this kind of powdered mixture.

4.3. Magnetic properties

Figure 5 represents the magnetization-field (M–H) hysteresis loops recorded at room temperature under varying magnetic field up to 1 T, and the inset shows M–H curves at low magnetic field. The M–H curves exhibit a sigmoidal shape with a small hysteresis loop typical of soft magnetic behavior of the milled powder mixture.

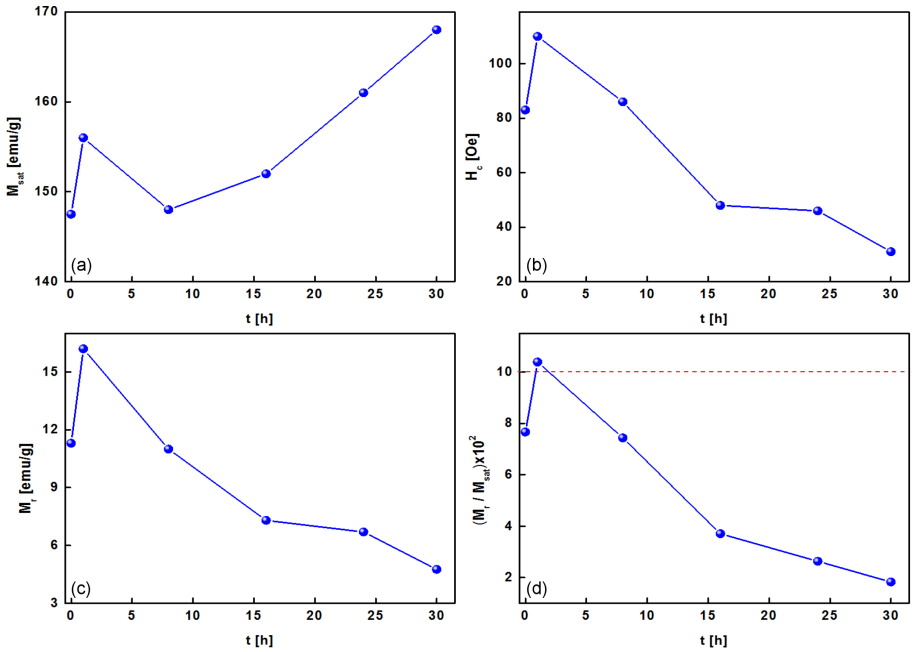

Fig. 6. Variation of (a) the saturation magnetization, (b) coercivity, (c) remanent magnetization, and (d) squareness ratio M_r/M_{sat} of the ball-milled $(Co_2Mn)_{40}Ni_{60}$ powder mixtures as a function of milling time.

Figure 6 displays the variation of the saturation magnetization $M_{\rm sat}$ (Fig. 6a), the coercivity H_c (Fig. 6b), the remanence M_r (Fig. 6c), and the squareness ratio $M_r/M_{\rm sat}$ (Fig. 6d) as a function of the milling time. It is well known that the values of $M_{\rm sat}$, H_c, and M_r are dependent on the chemical composition, crystallite size, magnetic anisotropy, stress, and temperature. For the milling time range (1–8 h), $M_{\rm sat}$ decreases, then rises and attains a maximum value of ≈ 170 emu/g at 30 h. The value of $M_{\rm sat}$ is mainly dependent on the individual magnetic moments of the constituent elements; i.e. Co (2.49 $\mu_{\rm B}$), Mn (2.7 $\mu_{\rm B}$), and Ni (1.26 $\mu_{\rm B}$). The increase of $M_{\rm sat}$ may be attributed to the enrichment of Ni and/or Co lattices by Mn atoms. Thus, the solute Mn atoms dissolved into Ni and/or Co lattices have resulted from the diffusion process. Additionally, at the early stage of milling, the enhancement of the internal microstrain produces crystalline defects that may reduce the moment of the saturation magnetization.

However, the increase of the magnetization up to 8 h of milling can be related to the SS phase formation due to the simultaneous dissolution of Mn and/or Co with higher magnetic moments within the Ni host lattice thereby enhancing the ferromagnetic ordering of the particles. As the coercivity and remanence depend significantly on the crystallite size [12], after 1 h of milling, the coercivity rises up to ≈ 110 Oe, and then declines with prolonged milling time to ≈ 31 Oe (30 h). It is well-known that the increase of H_c may be associated with heavy plastic deformations occurring during the milling process which introduce internal stress that can cause the motion of the pinning sites of the magnetic domain walls. Besides, the powder mixture can behave as a heterogeneous ferromagnetic system since the ball-milled powder at 1 h has three phases (Ni, hcp-Co and Mn as shown in Table I). The shape of particles and/or the surface roughness involved during the first stage of milling may lead to the increase of H_c. However, the decrease of the coercivity may be ascribed to the decrease of the large-sized lengths of particles. The remanence magnetization M_r increases within 1 h of milling, then decreases for an extending time (Fig. 6c). The variation of M_r may be associated with the changes in the particles' magnetic state. The $M_r/M_{\rm sat}$ ratio is a powerful domain state's criterion, namely single domains SD and multi-domains MD. One observes that the $M_r/M_{\rm sat}$ values are less than 0.105 (Fig. 6d). Therefore, the powder particles can be considered as multi-domains.

4.4. Approach to magnetic saturation

The approximation to saturation in the magnetization curves ($M \geq 0.95\ Ms$) for powders can be described by the following empirical law [23, 24]:

$$M(H) = M_0\left(1 - \frac{a_{1/2}}{(H+H_u+H_{ex})^{1/2}} - \frac{a_2}{H+H_u+H_{ex}}\right), \quad (1)$$

where H is the applied magnetic field, M_0 is the saturation magnetization, H_u is the coherent anisotropy field, and H_{ex} is the exchange field. The $a_{1/2}$ exponent is related to the structural defects and a_2 is linked to the intrinsic fluctuations.

TABLE II

Magnetic parameters (a_2, $H_{ex}+H_u$, $a_{1/2}$, H_{ex}, H_u, H_r, λ, and K_1) extracted from the approach to magnetic saturation.

t [h]	a_2 [kOe^2]	$H_{ex}+H_u$ [kOe]	$a_{1/2}$ [$kOe^{1/2}$]	H_{ex} [kOe]	H_u [kOe]	H_r [Oe]	λ	K_1 [10^5 erg/cm^3]
0	9.1	3.5	452.7	5.4	−1.9	369.3	25.0	26.8
1	4.0	2.4	762.2	3.0	−0.6	245.5	29.6	18.5
8	2.6	1.5	728.6	2.3	−0.8	198.0	30.8	14.5
16	2.6	1.5	728.6	2.3	−0.8	197.9	30.8	15.7
24	0.7	0.7	766.2	0.9	−0.2	103.7	39.6	8.7
30	0.6	0.2	684.8	0.9	−0.7	97.7	37.5	8.4

The disorder term, represented by $\frac{a_{1/2}}{(H+H_u+H_{ex})^{1/2}}$, can originate from the point-like defects, intrinsic magnetostatic variations or haphazardly distributed magnetic anisotropy [25]. The mutual magnetoelastic action of quasi-dislocation dipoles is expressed by $\frac{a_2}{H+H_u+H_{ex}}$ term.

Figure 7 shows the magnetization plots near saturation for $(Co_2Mn)_{40}Ni_{60}$ powder mixture at different milling time. Several parameters such as the anisotropy field H_r, the random local anisotropy constant K_1, and the coefficient λ have been extracted. Their relations are described with the following three equations:

$$H_{ex} = \left(\frac{a_2}{a_{1/2}}\right)^{2/3}, \tag{2}$$

$$a_{1/2} = \frac{H_r^2}{15H_{ex}^{3/2}}, \tag{3}$$

$$a_2 = \frac{H_r^2}{15} = \frac{1}{15}\left(\frac{2K_1}{M_s}\right)^2. \tag{4}$$

and their values are listed in Table II. The dimensionless coefficient λ is an important parameter to discern the difference between a strong anisotropy ($\lambda > 1$) and a weak one ($\lambda < 1$). It can be estimated using the following expression:

$$\lambda = \left(\frac{2}{15}\right)^{1/2}\frac{H_r}{H_{ex}}. \tag{5}$$

One can observe that the random local anisotropy constant K_1 decreases with increasing the milling time. The obtained values of λ, that are above 1, correspond to a heterogeneous ferromagnetic compound with strong random anisotropy.

4.5. Density functional theory calculation

The application of the KKR-CPA method was appropriate for $(Co_2Mn)_{40}Ni_{60}$ powder mixture considered as a chemical disordered system. Therefore, the total density of states (DOS) generated from this method is given in Fig. 8a. One can observe that the total DOS is mainly governed by Ni and Co contribution since their concentrations are higher than Mn.

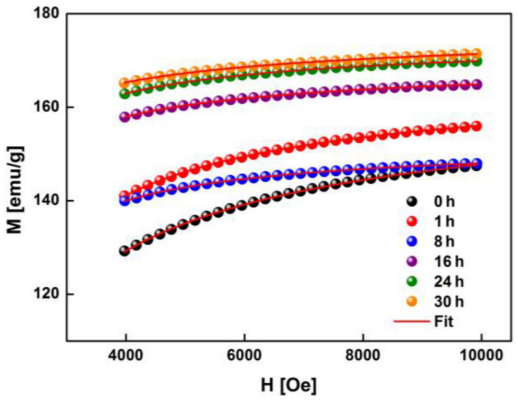

Fig. 7. Variation of the magnetization as a function of the applied magnetic field recorded for different milling times. The symbols represent the experimental data and the solid lines are the calculated values obtained from (1).

Moreover, it reveals an asymmetrical feature with respect to the energy axis, which identifies a magnetic system. The Fermi level, shown by a vertical dot-line, presents no zero DOS, featuring a metallic character of the studied powder mixture. The calculated magnetic moments of the constituting elements in the as-formed SS phase (Mn, Co, Ni) are as follows: 1.66 μ_B for Co, 2.65 μ_B for Mn and 0.69 μ_B for Ni. It can be noticed that the above values are relatively lower as compared to the empirical values (2.49 μ_B for Co, 2.7 μ_B for Mn, and 1.26 μ_B for Ni). This may be ascribed to the local arrangement of Co, Mn and Ni atoms within the fcc SS phase, resulting in anisotropic interactions, i.e., a disordered fcc phase compared to order structures of individual elements. The total magnetization of the disordered $(Co_2Mn)_{40}Ni_{60}$ powder mixture is found to be 1.16 μ_B and in excellent agreement with the experimental data (1.18 μ_B). The total magnetization's result of the disordered $(Co_2Mn)_{40}Ni_{60}$ powder mixture is found to be 1.16 μ_B in excellent agreement with the experimental data (1.18 μ_B).

Figure 8b–d illustrates the decomposed DOS of *s*-, *p*- and *d*- states of Co, Mn and Ni atoms. One can notice that the total DOS is mainly due to

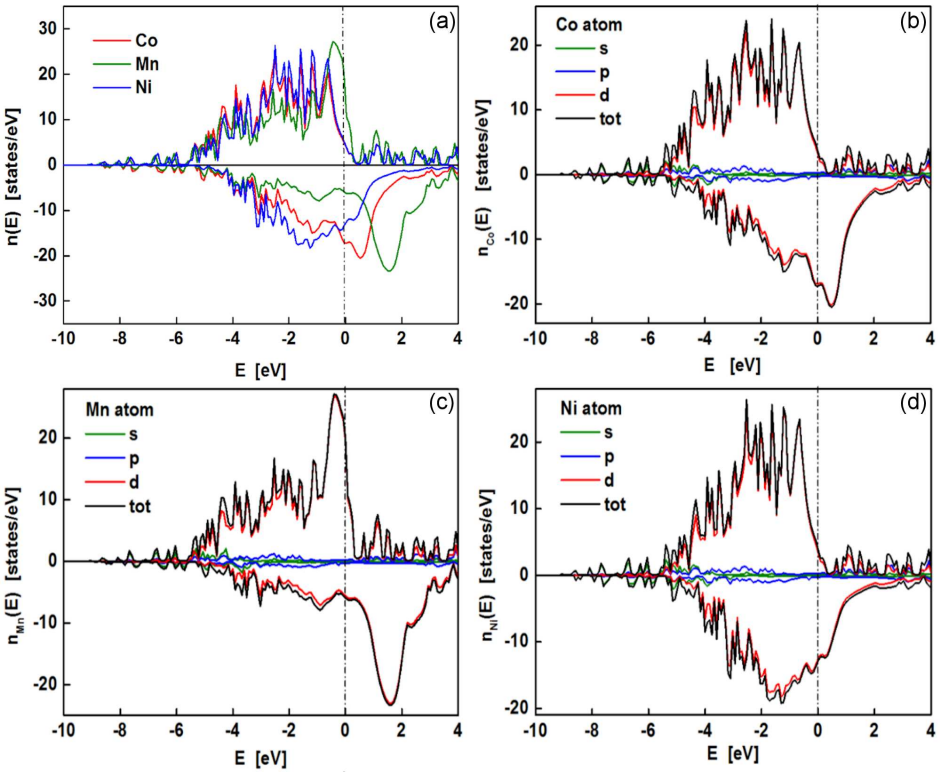

Fig. 8. (a) Total DOS of the disordered $(Co_2Mn)_{40}Ni_{60}$ powders estimated by using KKR-CPA method, and decomposed DOS of (s, p, d)-states for (b) Co, (c) Mn, and (d) Ni atoms estimated by using KKR-CPA method.

the 3d-like combined states, knowing that the spin of magnetic moment is not neglected in transition metals. Indeed, 3d-Co and 3d-Ni bands take part in the valence band, while the 3d-Mn band takes part in both occupied and unoccupied states near the Fermi level.

5. Conclusion

Nanocrystalline $(Co_2Mn)_{40}Ni_{60}$ powder mixture was prepared by mechanical alloying by means of high energy ball mill P7. After 16 h of milling, XRD analysis confirmed the formation of a single fcc-solid solution phase considered as a chemically disordered system. The microstructure study of the as-formed fcc-solid solution shows a reduction of the crystallite size accompanied by an increase in the microstrains for further milling. Magnetic measurements indicated a ferromagnetic behavior of a typical soft magnetic material, characterized by a strong anisotropy and the magnetic properties were found to be dependent upon the milling time. The approach to saturation magnetization manifested a decrease in the random local anisotropy constant K_1 with increasing the milling time. The total DOS is mainly due to the 3d-like states of both Co and Ni atoms. Because of the narrow coercivity, the as-fabricated nanocrystalline alloy can be used for magnetic amps.

Acknowledgments

The Ministère de l'Enseignement Supérieur et de la Recherche Scientifique Algérien and l'Ecole Nationale Supérieure des Mines et Métallurgie d'Annaba (ENSMM) are gratefully acknowledged.

References

[1] C.A. Ross, *Rev. Mater. Res.* **31**, 203 (2001).

[2] S.H. Tan, N.T. Nguyen, *Phys. Rev. E* **84**, 036317 (2011).

[3] A. Szpak, S. Fiejdasz, W. Prendota, T. Strączek, C. Kapusta, J. Szmyd, M. Nowakowska, S. Zapotoczny, *J. Nanopart. Res.* **16**, 2678 (2014).

[4] T. Bachaga, J. Zhang, M. Khitouni, J.J. Suñol, *Int. J. Adv. Manufact. Technol.* **103**, 2761 (2019).

[5] R.I. Jaffee, *J. Appl. Phys.* **19**, 867 (1948).

[6] Z. Zhu, X. Li, D. Zhu, *Mater. Manuf. Process.* **28**, 1301 (2013).

[7] M. Acet, C. John, E.F. Wassermann, *J. Appl. Phys.* **70**, 6556 (1991).

[8] H. Iijima, O. Taguchi, K.-I. Hirano, *Metall. Mater. Trans. A* **8**, 991 (1977).

[9] Y. Liu, H. Yang, G. Tan, Sh. Miyazaki, B. Jiang, Y. Liu, *J. Alloys Compd.* **368**, 157 (2004).

[10] N. Loudjani, N. Bensebaa, L. Dekhil, S. Alleg, J.J. Suñol, *J. Magn. Magn. Mater.* **323**, 3063 (2011).

[11] Y. Zhou, P. Nash, X. Dai, D. Li, A.A. Silva, G.R. Lopes Cardoso, *J. Alloys Compd.* **777**, 1274 (2019).

[12] S. Souilah, S. Alleg, M. Bououdina, J.J. Suñol, E.K. Hlil, *J. Supercond. Nov. Magn.* **30**, 1927 (2017).

[13] H. Moumeni, A. Nemamcha, S. Alleg, J.M. Grenèche, *Mater. Chem. Phys.* **138**, 209 (2013).

[14] L. Dekhil, S. Alleg, M. Bououdina, J.J. Suñol, J.M. Grenèche, *Adv. Powder Technol.* **26**, 519 (2015).

[15] V.M. Antonov, Y. Dorofeev, V.A. Kazantsev, A. Shikov, A. Teplykh, *Sov. Phys. JETP* **67**, 336 (1988).

[16] S. Ōhara, S. Komura, T. Takeda, T. Hihara, Y. Komura, *J. Phys. Soc. Jpn.* **42**, 1881 (1977).

[17] G.Y. Qiao, F.R. Xiao, J. Yang, L.N. Sun, L.J. Guo, T.F. Jing, *Mater. Manufact. Process.* **27**, 1154 (2012).

[18] H. Akai, *J. Phys. Condens. Matter* **1**, 8045 (1989).

[19] S.H. Vosko, L. Wilk, M. Nusair, *Can. J. Phys.* **58**, 1200 (1980).

[20] H. Akai, MACHIKANEYAMA2002V08, Osaka University, Japan.

[21] L. Lutterotti, S. Matthies, H.R. Wenk, "MAUD — A Friendly Java Program for Material Analysis Using Diffraction", Newslett. CPD **21**, 14 (1999).

[22] W. Laslouni, Z. Hamlati, M. Azzaz, *Acta Phys. Pol. A* **128**, B-190 (2015).

[23] H. Kronmuller, *IEEE Trans. Magn.* **15**, 1218 (1979).

[24] E. Loudghiri, A. Belayachi, N. Hassanain, O. Touraghe, A. Hassini, H. Lassri, *Phys. Lett. A* **371**, 504 (2007).

[25] A. Neuweiler, B. Hofmann, H. Kronmüller, *J. Magn. Magn. Mater.* **153**, 28 (1996).